

AD-A228 102

REPORT DOCUMENTATION PAGE

Form Approved
OMB No. 0704-0188

2

Public reporting burden for this collection of information is estimated to average 1 hour per response, including the time for reviewing instructions, searching existing data sources, gathering and maintaining the data needed, and completing and reviewing the collection of information. Send comments regarding this burden estimate or any other aspect of this collection of information, including suggestions for reducing this burden, to Washington Headquarters Services, Directorate for Information Operations and Reports, 1215 Jefferson Davis Highway, Suite 1204, Arlington, VA 22202-4302, and to the Office of Management and Budget, Paperwork Reduction Project (0704-0188), Washington, DC 20503

1. AGENCY USE ONLY (Leave blank) 2. REPORT DATE
6 Jun 88 3. REPORT TYPE AND DATES COVERED
Conference Presentation

4. TITLE AND SUBTITLE
Unsteady Aerodynamic Forces at Low Airfoil Pitching Rates 5. FUNDING NUMBERS
TA 2307-F1-38

6. AUTHOR(S)
J. Albertson, T. Troutt, C. Kedzie

7. PERFORMING ORGANIZATION NAME(S) AND ADDRESS(ES)
F.J. Seiler Research Laboratory
USAF Academy CO 80840-6528 8. PERFORMING ORGANIZATION REPORT NUMBER
FJSRL-PR-90-0015

9. SPONSORING, MONITORING AGENCY NAME(S) AND ADDRESS(ES) 10. SPONSORING, MONITORING AGENCY REPORT NUMBER

DTIC
ELECTE
OCT 31 1990
S E D

11. SUPPLEMENTARY NOTES

12a. DISTRIBUTION / AVAILABILITY STATEMENT
Distribution Unlimited 12b. DISTRIBUTION CODE

13. ABSTRACT (Maximum 200 words)
Experiments were conducted on a NACA-0015 airfoil undergoing low constant pitch rates to study the effects of dynamic stall formation on the airfoil upper surface pressure field. The airfoil was pitched about pivot locations of 0.25c, 0.5c, and 0.75c at nondimensional pitch rates below 0.2. Lift and drag coefficients were evaluated for all cases, and smoke flow visualization at low pitch rates was studied for the quarter chord pivot location. Results indicate that the greatest increases in lift due to the pitching motion occur prior to the nondimensional pitch rate of 0.1 for all three pivot locations. The effects of pitch rate on the maximum lift and drag values appear similar for the three pivot locations studied. Lift to drag ratios show significant enhancement even at very low nondimensional pitch rates. Flow visualization indicates that the leading edge dynamic stall vortex is present even at very low nondimensional pitch rates. Keywords: Aerodynamic lift/drag; Pitch motion; Airfoils; Leading edges; Stall vortices;

14. SUBJECT TERMS
flow visualization
aerodynamic forces;
unsteady flow; Reprints. (CEDC) ← 15. NUMBER OF PAGES
9 16. PRICE CODE

17. SECURITY CLASSIFICATION OF REPORT
UNCLASSIFIED 18. SECURITY CLASSIFICATION OF THIS PAGE
UNCLASSIFIED 19. SECURITY CLASSIFICATION OF ABSTRACT
UNCLASSIFIED 20. LIMITATION OF ABSTRACT
NONE

DUPLICATE COPY

A

UNSTEADY AERODYNAMIC FORCES AT LOW AIRFOIL PITCHING RATES

Julie A. Albertson*
and
Timothy R. Troutt**

Department of Mechanical and Materials Engineering
Pullman, WA 99164-2920

Christopher R. Kedzie***

Frank J. Seiler Research Laboratory
USAF Academy, Colorado Springs, CO 80840-6528

Abstract

Experiments were conducted on a NACA-0015 airfoil undergoing low constant pitch rates to study the effects of dynamic stall formation on the airfoil upper surface pressure field. The airfoil was pitched about pivot locations of 0.25c, 0.50c, and 0.75c at nondimensional pitch rates, α^+ , below 0.2. Lift and drag coefficients were evaluated for all cases, and smoke flow visualization at low pitch rates was studied for the quarter chord pivot location. Results indicate that the greatest increases in lift due to the pitching motion occur prior to the nondimensional pitch rate of 0.1 for all three pivot locations. The effects of pitch rate on the maximum lift and drag values appear similar for the three pivot locations studied. Lift to drag ratios show significant enhancement even at very low nondimensional pitch rates. Flow visualization indicates that the leading edge dynamic stall vortex is present even at very low nondimensional pitch rates.

Nomenclature

c	airfoil chord
C_d	airfoil pressure drag coefficient
C_l	airfoil lift coefficient
L/D	airfoil lift to drag ratio = C_l/C_D
Re	chord Reynolds number = $\frac{U_\infty c}{\nu}$
U_∞	freestream velocity
$\dot{\alpha}$	pitch rate
α^+	nondimensional pitch rate = $\frac{\dot{\alpha} c}{U_\infty}$
ν	kinematic viscosity

Introduction

The flow phenomena associated with unsteady airfoil motion have been a major research focus for the past two decades.¹ Specific attention has been given to dynamic stall and its associated effects on the airfoil surface pressure field.^{2,3} The enhanced aerodynamic forces resulting from pitching motions may lead to improved maneuverability of high-performance aircraft.⁴

The phenomena of dynamic stall occurs when airfoils are pitch up rapidly beyond their static stall angle of attack. As the angle of attack increases, the flow separates and a region of vorticity develops. The dynamic stall vortex forms near the airfoil leading edge, grows as the airfoil continues its upward motion, and eventually moves along the airfoil surface and detaches. Numerous studies have been done on sinusoidally oscillating airfoils to analyze the dynamic stall vortex characteristics and the corresponding pressure field.^{5,6,7,8}

Recent experimental studies have concentrated on the simpler case of airfoils undergoing constant pitching motions. These investigations have focused on the developing unsteady aerodynamic forces and the dynamic stall phenomena occurring on the surface. Dramatic increases in lift and drag from corresponding maximum static levels occur over a wide range of nondimensional pitch rates, α^+ .^{9,10,11} Flow visualization studies have also shown direct correlations between the dynamic stall vortex and the upper surface pressure field.^{12,13,14}

Experimental results are presented here to clarify the effects of pivot locations on airfoil performance at relatively low nondimensional pitch rates. The concentration on low nondimensional pitch rates pursued in this work stems from previous experimental observations that the dependence of unsteady aerodynamic forces on pitch rate is especially strong in this region.¹⁵ This is one of the first attempts to correlate the effect of pivot location on the unsteady aerodynamic forces at these low nondimensional pitch rates. In addition, the influence of pitching motion and pivot location on lift to drag ratios is explored to determine relationships between

* Research Assistant, Student Member AIAA

** Associate Professor, Member AIAA

*** Research Associate

the upper surface pressure field on the airfoil and the dynamic stall phenomena. The associated behavior of the dynamic stall vortex at low nondimensional pitch rates is also examined using flow visualization results.

Experimental Methods

The experiments discussed here were conducted at the U.S. Air Force Academy in the Frank J. Seiler Research Laboratory's 0.91 m x 0.91 m low speed wind tunnel. The model used was a NACA 0015 airfoil with a 15 cm chord and a 58 cm span. The airfoil was pitched at a constant rate from 0° to 60° around pivot locations of 25%, 50% and 75% of the chord. The airfoil motion was accomplished using a stepper motor assembly controlled by a MASSCOMP 5500 micro-computer system. Instantaneous surface pressure measurements were made using eighteen Endevco 8507-2 miniature pressure transducers mounted in close-coupled connection to surface pressure ports.

Flow visualization was obtained using a 0.013 cm diameter tungsten wire located 30 cm upstream of the airfoil leading edge and perpendicular to the airfoil span. A smoke producing oil was coated on the wire and then heated electrically to create uniform streaklines. High speed movies were taken with a LOCAM II 16 mm high speed movie camera operating at 200 frames per second. Illumination was provided by three Strobrite stroboscopic lights synchronized with the camera. Pressure measurements were taken with a tunnel speed of 7.62 m/s, corresponding to a chord Reynolds number of 60000, while flow visualization was done with a tunnel speed of 6.10 m/s, corresponding to a chord Reynolds number of 47000, allowing higher resolution. A range of nondimensional pitch rates α^+ , from 0 to 0.2 was evaluated in detail. It has been shown previously that α^+ can be treated as a similarity parameter in flows such as the one studied here.¹⁶

Experimental Results

Pressure Measurements

The change in lift coefficient with respect to angle of attack is presented for the quarter chord pivot location in figure 1 at nondimensional pitch rates, α^+ between 0 and 0.15. A significant increase in maximum lift coefficient from the static case is evident even at an α^+ of 0.03. Maximum lift coefficients continue to increase for the subsequent α^+ values of 0.1 and 0.15, although the differential between maximum lift coefficients diminishes as the nondimensional pitch rate increases.

The angle of attack at which maximum lift occurs also increases as the nondimensional pitch rate grows. Two peaks are apparent in the lift coefficient curve at $\alpha^+ = 0.03$, with the greatest lift value for that pitch rate occurring at the first peak. Only one significant peak is evident at α^+ values of 0.1 and 0.15. There are slight peaks in the $\alpha^+ = 0.03$ and 0.1 curves at attack angles higher than the maximum lift angles, but it be noted that these peaks are not greater than the experimental error.

The relationship between the maximum lift coefficients and the nondimensional pitch rate is shown in figure 2 for three different pivot locations. The behavior of the maximum lift coefficient with respect to α^+ is similar for the three pivot locations. Maximum lift values increase rapidly between $\alpha^+ = 0$ and 0.05, and then level off for the remainder of the pitch rate range studied. This finding is similar to results reported by Francis and Keese¹⁷ concerning airfoils pitching in a similar α^+ range with pivot locations of 0.32c and 0.38c. Maximum lift coefficients are equal within the indicated errors for all three pivot locations.

The relationship between the drag coefficient and the attack angle corresponding to α^+ values between 0 and 0.15 is given in figure 3 for the 0.25c pivot location. Two peaks are apparent in the $\alpha^+ = 0.03$ curve, with the latter peak being slightly higher in magnitude than the first. Two peaks are again evident in the curve for $\alpha^+ = 0.1$, although in this case it is the first peak which coincides with the maximum drag. Only one peak occurs in the curve at $\alpha^+ = 0.15$. The magnitude of the maximum drag coefficient and the attack angle at which it occurs increases with increasing nondimensional pitch rate for the four pitch rates shown.

The relationship between the maximum drag coefficient and the nondimensional pitch rate can also be seen in figure 4. All three pivot locations follow the same trend although values for the 0.50c pivot location deviate slightly from patterns followed by the other two cases between $\alpha^+ = 0.075$ and 0.15. The maximum drag coefficients increase rapidly to a local maximum at $\alpha^+ = 0.075$ for all three pivot locations. Values gradually increase again between $\alpha^+ = 0.1$ and 0.2.

The attack angles coinciding to the maximum lift and drag coefficients as a function of α^+ are shown in figure 5 for pitching about the quarter chord. The attack angle corresponding to maximum lift curve exhibits behavior similar to the maximum lift curve shown in figure 2. The maximum lift attack angle increases between $\alpha^+ = 0$ and 0.075, and then begins to level off. The attack angle corresponding to peak drag follows the same trend as the peak drag curve shown in figure 4. The maximum drag attack angle increases rapidly between $\alpha^+ = 0$ and 0.075, decreases between α^+ values of 0.075 and 0.1, and then begins to increase in a manner similar to the maximum lift attack angles. The attack angles corresponding to maximum drag coefficient are significantly higher than those coinciding to maximum lift coefficient between α^+ values of 0.03 and 0.1.

The effects of pitching motion and pivot location on the airfoil lift to drag ratios were also evaluated. Lift to drag ratios as a function of attack angle for the quarter chord pivot location are shown in figure 6 at the nondimensional pitch rates of 0, 0.02, and 0.1. Values for the static case are greater than those for the two dynamic cases between attack angles of 0° and 14°, where 14° corresponds approximately to static stall. Lift to drag ratios for the static case drop off rapidly after stall, but lift to drag ratios at corresponding attack angles for the dynamic cases are higher than the static ratios. The range over which lift to drag ratios are greater than the static case increases with increasing pitch rate. Although exact values cannot be determined due to experimental errors, an increase in lift to drag ratios for the dynamic cases over values for the static case is clearly evident. Both the curve at $\alpha^+ = 0.02$ and at $\alpha^+ = 0.1$ asymptote towards the static values later in the pitching cycle.

Figure 7 shows lift to drag ratios as a function of nondimensional pitch rate.



or

lon

n/

ity Codes

and/or

Dist special

A-1

mensional pitch rate for attack angles between 5° and 20° . The highest overall lift to drag ratios occur at $\alpha = 5^\circ$, with values at this attack angle being approximately constant between $\alpha^+ = 0.005$ and 0.1 , and then decreasing. For an attack angle of $\alpha = 15^\circ$ lift to drag ratios are approximately constant between $\alpha^+ = 0.005$ and 0.075 and then begin to decrease. For the attack angle $\alpha = 15^\circ$ lift to drag ratios increase rapidly between $\alpha^+ = 0$ and 0.005 and then remain constant for the higher pitch rates. Values for $\alpha = 20^\circ$ show a slight increasing trend between $\alpha^+ = 0$ and 0.02 and then become constant. It should be noted for attack angles of 5° and 10° that initial lift to drag ratios decrease from the static case, $\alpha^+ = 0$, to the dynamic case of $\alpha^+ = 0.005$, whereas they increase in this range for an attack angle of 15° . This is caused by the occurrence of static stall near $\alpha = 14^\circ$ and the subsequent drop in static lift to drag ratios.

An evaluation was also made to determine the effect of pivot location on lift to drag ratios. Graphs for $\alpha^+ = 0.02$ and 0.1 are shown in Figures 8a and 8b respectively. Prior to $\alpha = 14^\circ$, lift to drag ratios are slightly lower for the $0.25c$ and $0.75c$ pivot points than the $0.50c$ case at an α^+ of 0.02 , shown in figure 8a. Lift to drag values for the $0.75c$ pivot location are the lowest of the three pivot cases in this region. This trend continues for the case of $\alpha^+ = 0.1$, given in figure 8b. Lift to drag ratios for the $0.75c$ pivot location are consistently lower than the other two cases, and values for the $0.50c$ pivot locations are higher than those for $0.25c$ and $0.75c$ positions prior to $\alpha = 20^\circ$. Lift to drag ratios are similar for all three pivot locations for attack angles greater than $\alpha = 20^\circ$.

Flow Visualization

Smoke flow visualization for the quarter chord pivot point is shown in figure 9 for $\alpha^+ = 0.01$. The flow appears symmetric at $\alpha = 5^\circ$. At $\alpha = 10^\circ$, a separation region has formed near the trailing edge and is moving upstream. The flow is separated over a large percentage of the airfoil surface at $\alpha = 15^\circ$. A loosely defined dynamic stall vortex covering virtually the entire upper surface is clearly evident at $\alpha = 20^\circ$. Unfortunately, the flow visualization methods used in this experiment did not allow flow observations at higher attack angles for this nondimensional pitch rate.

Flow visualization for $\alpha^+ = 0.03$ is presented in figure 10 for the quarter chord pivot point. The flow follows a similar pattern as $\alpha^+ = 0.01$, although respective changes occur slightly later in the pitching cycle. A separation region is beginning to grow at $\alpha = 15^\circ$, and covers a greater portion of the airfoil surface at $\alpha = 20^\circ$. Close observation at this attack angle also reveals evidence of a dynamic stall vortex forming at the leading edge. This vortex is even more evident at $\alpha = 25^\circ$, and covers approximately half of the airfoil chord. Between angles of attack of 25° and 30° the dynamic stall vortex is disrupted by a counter-clockwise vortex which forms at the airfoil trailing edge. At the attack angle of 30° shown in figure 10f, the dynamic stall vortex has detached from the airfoil surface and can be seen in the upper left hand corner of the figure. A second dynamic stall vortex is beginning to form at $\alpha = 30^\circ$, and covers the entire airfoil surface at $\alpha = 35^\circ$. This vortex is not as clearly defined and has a shorter surface residence time than the first vortex.

Flow visualization at $\alpha^+ = 0.05$, shown in figure 11, exhibits flow behavior similar to that at $\alpha^+ = 0.03$. The dy-

amic stall vortex can again be seen at $\alpha = 20^\circ$ by close observation, but its subsequent growth is noticeably delayed. At $\alpha = 25^\circ$, given in figure 11e, the dynamic stall vortex is clear but occupies a smaller surface region than it did for the corresponding attack angle for $\alpha^+ = 0.03$. The vortex is still involved with the airfoil surface at $\alpha = 30^\circ$, but has detached by $\alpha = 35^\circ$. A loose trailing edge vortex is evident at this attack angle, shown in figure 11g, and a second dynamic stall vortex appears to be forming.

The presence of more than one dynamic stall vortex at $\alpha^+ = 0.03$ and 0.05 seems to have a direct effect on the shape of the lift and drag coefficient curves, since the peaks in these curves coincide with the attack angles at which the dynamic stall vortex is apparent on the airfoil upper surface. It has been shown previously that movement of the dynamic stall vortices on the airfoil is closely connected to the aerodynamic forces generated, and that peaks in the drag coefficient with respect to attack angle curves correspond to detachment of the dynamic stall vortex from the airfoil surface.¹⁵

Conclusions

The results of this study indicate that the greatest enhancement of lift due to the constant pitching motion of the NACA-0015 airfoil occur at low nondimensional pitch rates, namely α^+ below 0.1 , for the three pivot points evaluated. The range of nondimensional pitch rates between $\alpha^+ = 0.03$ and 0.1 coincides with the region where the occurrence of maximum lift significantly precedes maximum drag in the pitching cycle. Lift to drag ratios were found to depend on pivot position, with values being consistently lower for the three-quarter chord pivot location than for the other two cases. It was found that lift to drag ratios are greater for the dynamic cases than the static case at high angles of attack. Flow visualization showed that the dynamic stall vortex is present even at a nondimensional pitch rate of 0.01 , and that the presence of subsequent vortices on the upper airfoil surface during the pitching cycle creates local maxima in the lift and drag coefficients.

Acknowledgements

This research was sponsored by the Air Force Office of Scientific Research/AFSC, United States Air Force, under Contract F49620-85-C-0013. The authors gratefully acknowledge the support of Major J.M. Walker and Dr. M.C. Robinson. They also thank Captain E. Stephen for his help with experimental preparations, and the support staff of the Frank J. Seiler Research Laboratory for general assistance with experimental facilities.

References

1. McCroskey, W.J., "Unsteady Airfoils," Ann Rev Fluid Mech 14, pp. 285-311, 1982.
2. Reynolds, W.C. and Carr, L.W., "Review of Unsteady, Driven, Separated Flows," AIAA Paper No. 85-0527, March 1985.

3. Gad-el-Hak, M., "Unsteady Separation on Lifting Surfaces," Appl. Mech. Rev., Vol. 40, No. 4, pp. 441-452, April 1987.
4. Herbst, W.B., "Supermaneuverability," Proceedings from Workshop on Unsteady Separated Flows, USAFA, Department of Aeronautical Engineering, University of Colorado, Boulder, CO, pp. 1-9, August 1983.
5. McAlister, K.W. and Carr, L.W., "Water Tunnel Visualizations of Dynamic Stall," J. Fluids Engr, 101, pp. 376-380, September 1979.
6. Adler, J.N., Robinson, M.C., Luttgies, M.W., and Kennedy, D.A., "Visualizing Unsteady Separated Flows," Flow Visualization III, Hemisphere Publishing, New York, pp. 342-347, 1985.
7. Robinson, M.C. and Luttgies, M.W., "Unsteady Flow Separation and Attachment Induced by Pitching Airfoils," AIAA Paper No. 83-0131, June 1983.
8. Gad-el-Hak, M. and Ho, C.M., "Three-Dimensional Effects on a Pitching Lifting Surface," AIAA Paper No. 85-0041, January 1985.
9. Walker, J.M., Helin, H.E. and Strickland, J.H., "An Experimental Investigation on an Airfoil Undergoing Large Amplitude Pitching Motions," AIAA Paper No. 85-0039, January 1985.
10. Jumper, E.J., Shreck, S.J., and Dimmick, R.L., "Lift-Curve Characteristics for an Airfoil Pitching at a Constant Rate," AIAA Paper No. 86-0117, January 1986.
11. Walker, J.M., and Chou, D.C., "Forced Unsteady Vortex Flows Driven by Pitching Airfoils," AIAA Paper No. 87-1331, January 1987.
12. Helin, H.E. and Walker, J.M., "Interrelated Effects of Pitch Rate and Pivot Point on Airfoil Dynamic Stall," AIAA Paper No. 85-0130, January 1985.
13. Strickland, J.H. and Graham, G.M., "Force Coefficients for a NACA-0015 Airfoil Undergoing Constant Pitch Rate Motions," AIAA J., Vol. 25, No. 4, pp. 622-624, April 1987.
14. Albertson, J.A., Troutt, T.R., Siuru, W.D., and Walker, J.M., "Dynamic Stall Vortex Development and the Surface Pressure Field of a Pitching Airfoil," AIAA Paper No. 87-1333, June 1987.
15. Walker, J.M., Helin, H.E., and Chou, D.C., "Unsteady Surface Pressure Measurements on a Pitching Airfoil," AIAA Paper No. 85-0532, March 1985.
16. Cook, R.J., "Similarity Conditions for Flows About Pitching Airfoils," FJSRL-TM-87-0003, June 1987.
17. Francis, M.S. and Keesee, J.E., "Airfoil Dynamic Stall Performance with Large Amplitude Motions," AIAA J., Vol. 23, No. 11, pp. 1653-1659, November 1985.

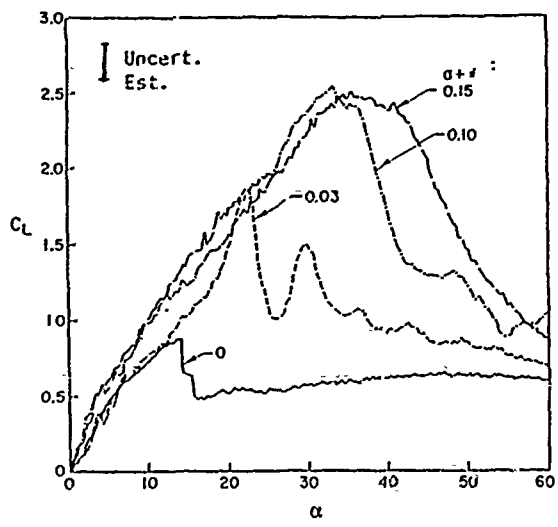


Figure 1. Lift coefficient as a function of attack angle. Pivot = 0.25c.

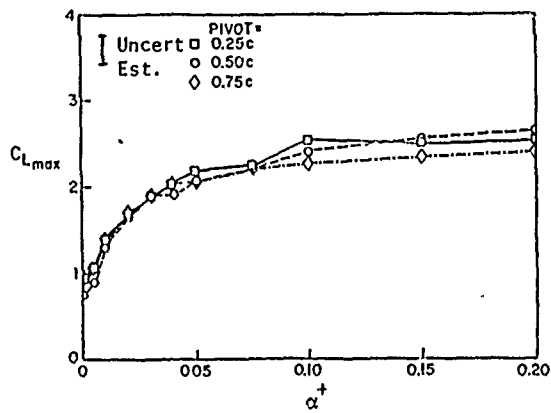


Figure 2. Maximum lift coefficient as a function nondimensional pitch rate.

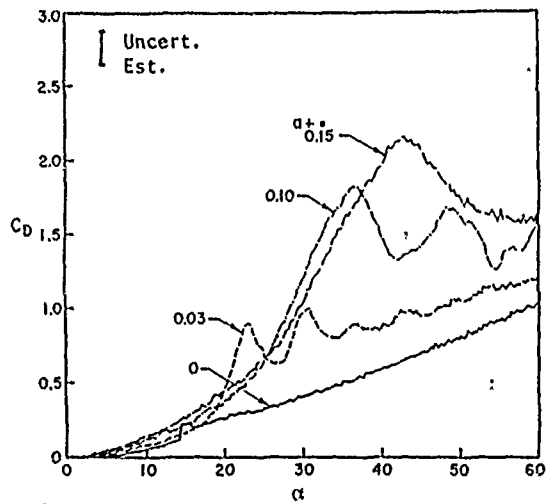


Figure 3. Drag coefficient as a function of attack angle. Pivot = 0.25c.

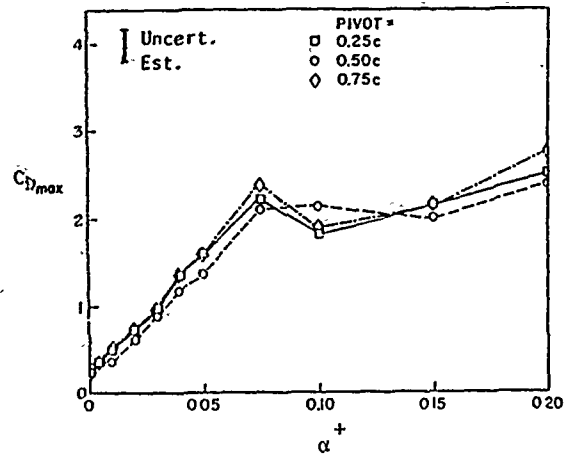


Figure 4. Maximum drag coefficient as a function of nondimensional pitch rate.

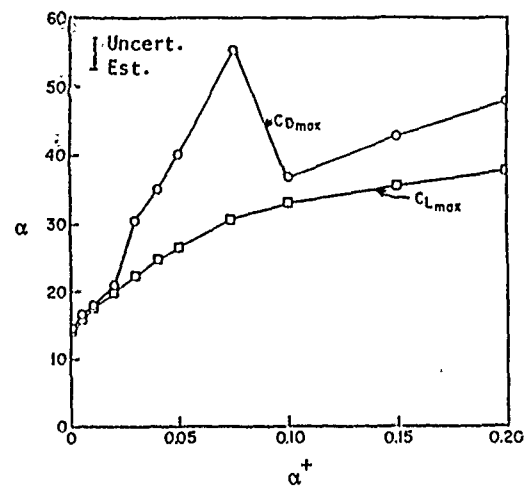


Figure 5. Angle of attack corresponding to maximum lift and drag coefficient as a function of nondimensional pitch rate. Pivot location = 0.25c.

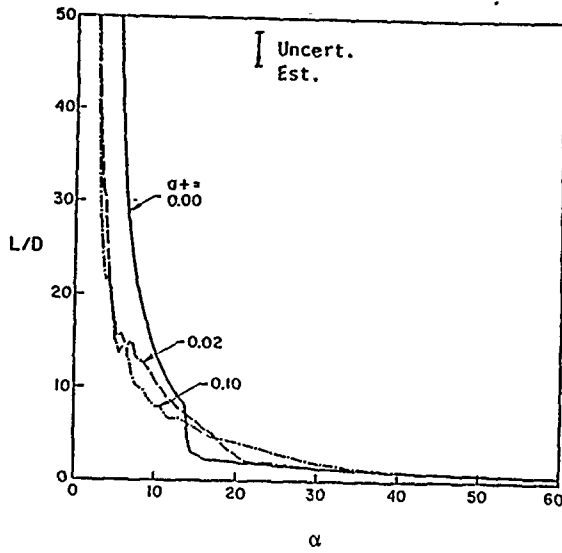
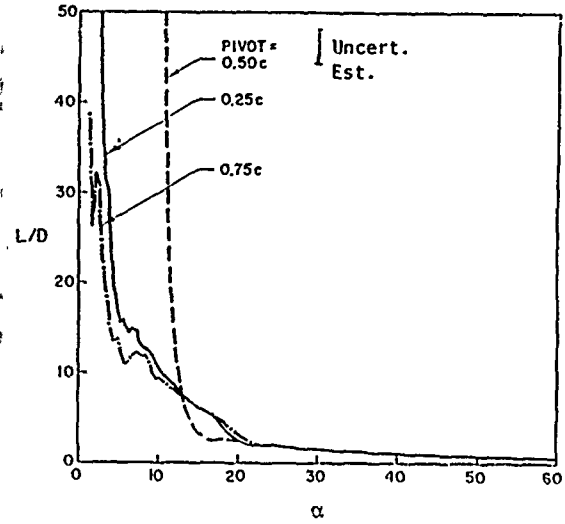


Figure 6. Lift to drag ratios as a function of attack angle. Pivot location = 0.25c.



a) $\alpha^+ = 0.02$

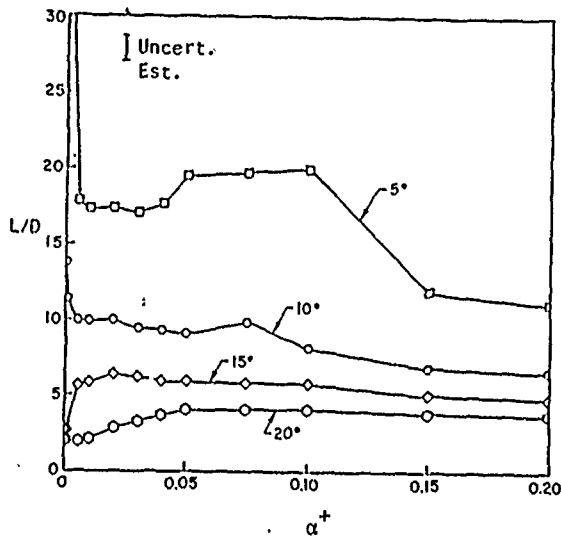
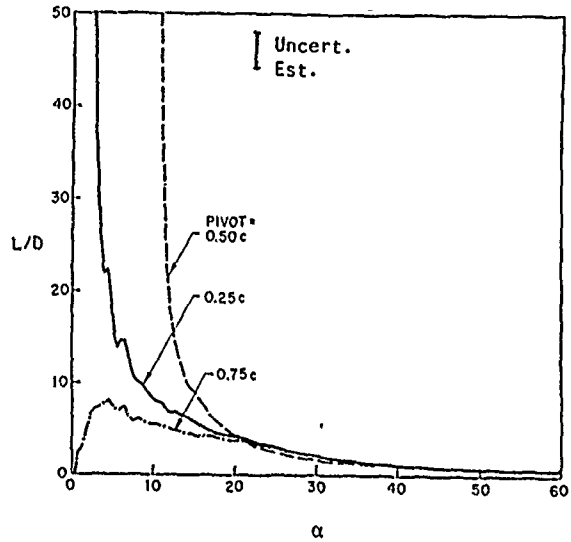
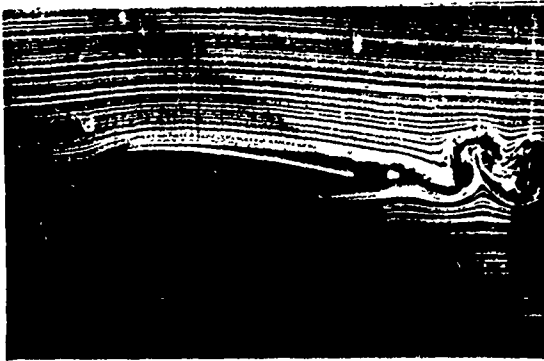


Figure 7. Lift to drag ratios as a function of nondimensional pitch rate. Pivot location = 0.25c.

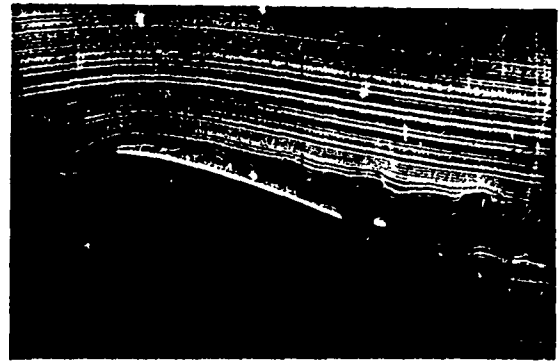


b) $\alpha^+ = 0.1$

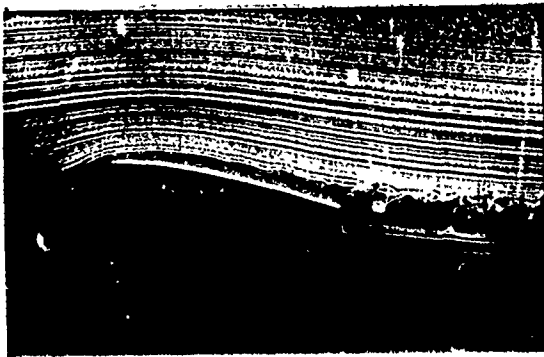
Figure 8. Lift to drag ratios as a function of attack angle.



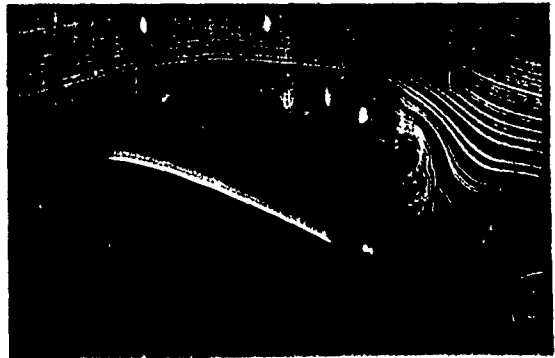
a) $\alpha = 5^\circ$



c) $\alpha = 15^\circ$

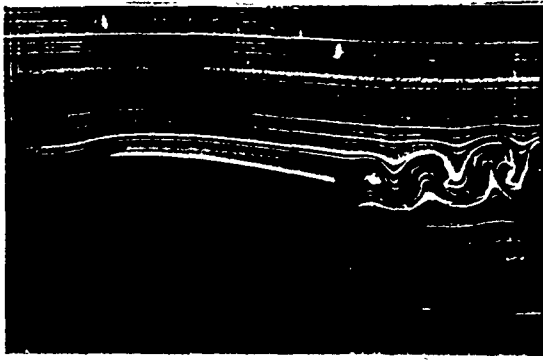


b) $\alpha = 10^\circ$



d) $\alpha = 20^\circ$

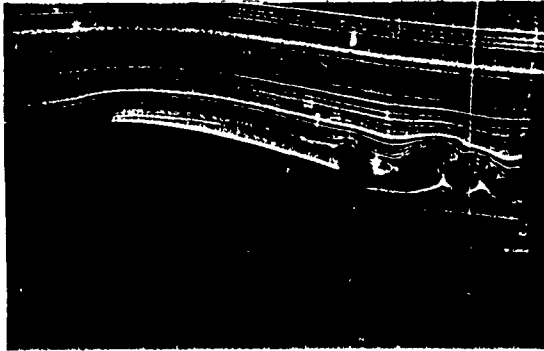
Figure 9. Smoke flow visualization. Pivot location = $0.25c$. $\alpha^+ = 0.01$.



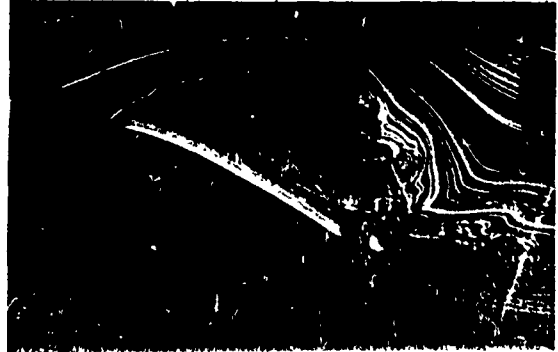
a) $\alpha = 5^\circ$



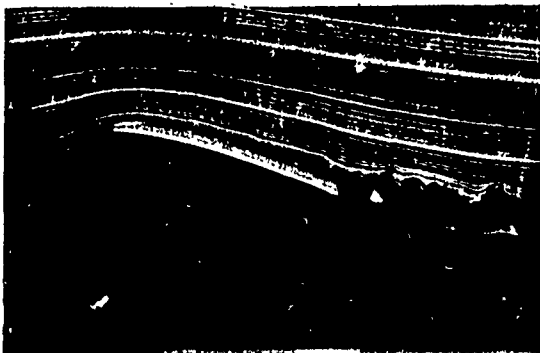
e) $\alpha = 25^\circ$



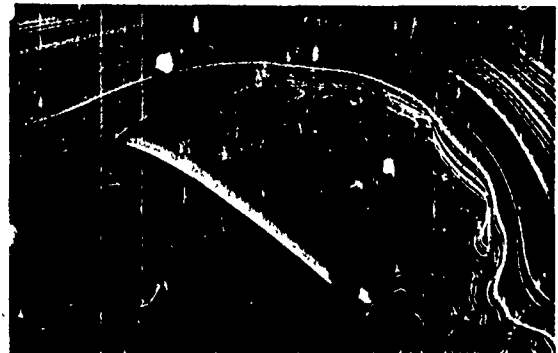
b) $\alpha = 10^\circ$



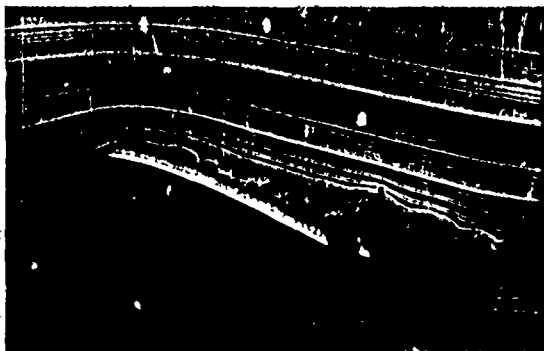
f) $\alpha = 30^\circ$



c) $\alpha = 15^\circ$



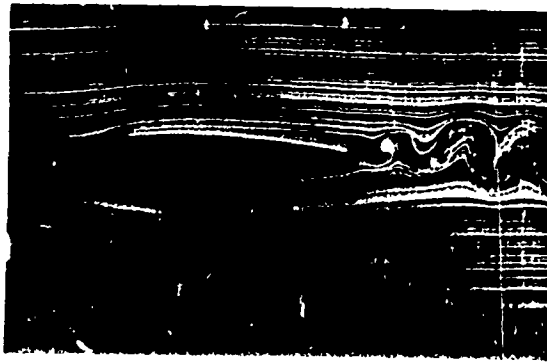
g) $\alpha = 35^\circ$



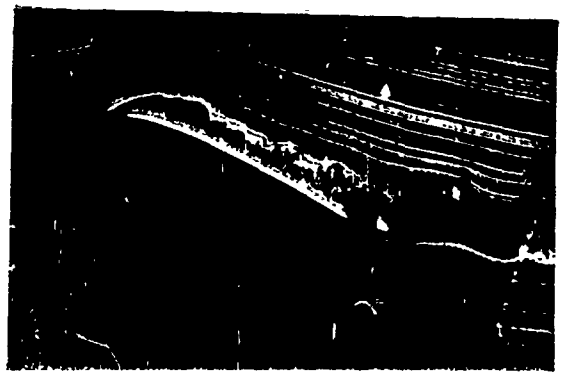
d) $\alpha = 20^\circ$

Figure 10. Smoke flow visualization. Pivot location = $0.25c$. $\alpha^+ = 0.03$.

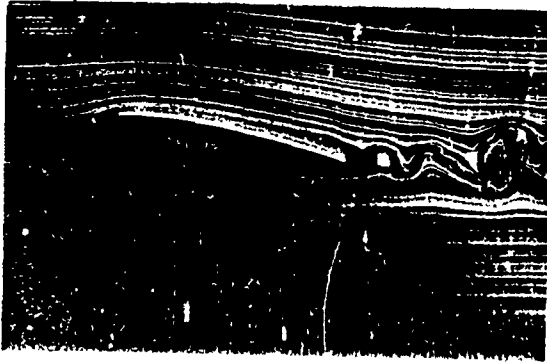
0 / 0 !



a) $\alpha = 5^\circ$



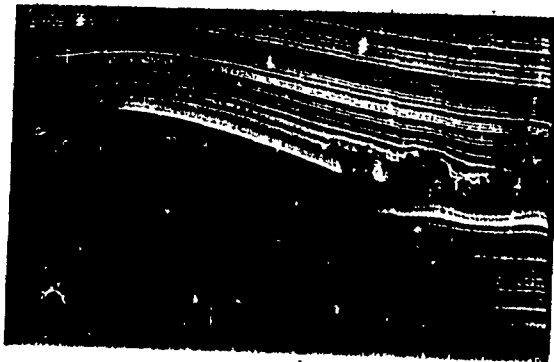
e) $\alpha = 25^\circ$



b) $\alpha = 10^\circ$



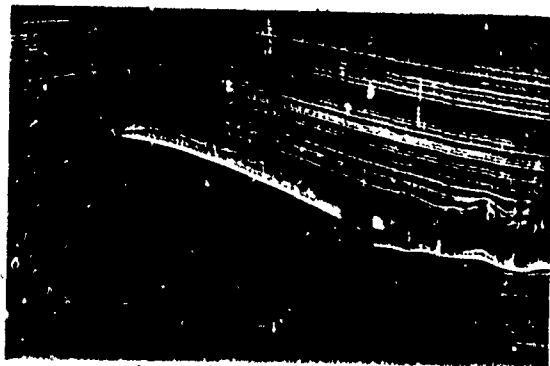
f) $\alpha = 30^\circ$



c) $\alpha = 15^\circ$



g) $\alpha = 35^\circ$



d) $\alpha = 20^\circ$

Figure 11. Smoke flow visualization. Pivot location = $0.25c$. $\alpha^+ = 0.05$.